



Article

Composition-Dependent Sorptive Fractionation of Anthropogenic Dissolved Organic Matter by Fe(III)-Montmorillonite

Robert B. Young ¹ , Shani Avneri-Katz ², Amy M. McKenna ³ , Huan Chen ³,
William Bahureksa ⁴, Tamara Polubesova ², Benny Chefetz ² and Thomas Borch ^{1,4,*}

¹ Department of Soil and Crop Sciences, Colorado State University, Fort Collins, CO 80523, USA; robert.b.young@colostate.edu

² Department of Soil and Water Sciences, Faculty of Agriculture, Food and Environment, The Hebrew University of Jerusalem, Rehovot 7610001, Israel; shani.avneri@mail.huji.ac.il (S.A.-K.); tamara.polubesova@mail.huji.ac.il (T.P.); benny.chefetz@mail.huji.ac.il (B.C.)

³ National High Magnetic Field Laboratory, Florida State University, Tallahassee, FL 32310, USA; mckenna@magnet.fsu.edu (A.M.M.); huan.chen@magnet.fsu.edu (H.C.)

⁴ Department of Chemistry, Colorado State University, Fort Collins, CO 80523, USA; William.Bahureksa@colostate.edu

* Correspondence: thomas.borch@colostate.edu; Tel.: +1-970-491-6235

Received: 1 December 2017; Accepted: 22 February 2018; Published: 2 March 2018

Abstract: Water transports organic matter through soils, where mineral-organic associations form to retain dissolved organic matter (“DOM”), influencing terrestrial carbon cycling, nutrient availability for plant growth, and other soil organic matter functions. We combined Fourier transform ion cyclotron resonance mass spectrometry with novel data analysis techniques to examine the role of sorptive fractionation in the associations between Fe(III)-montmorillonite and DOM from composted biosolids (“anthropogenic DOM”). To examine the influence of DOM composition on sorption and sorptive fractionation, we used resin-based separation to produce DOM subsamples with different molecular compositions and chemical properties. A large proportion (45 to 64%) of the initial carbon in every DOM solution sorbed to the Fe(III)-montmorillonite. However, when the compositions of the initial solutions were compared to the sorbed organic matter, the computed changes in composition were lower (10 to 32%). In fact, non-selective sorption was more important than selective sorption in every sample, except for the hydrophilic neutral (HiN) fraction, where high nitrogen content and acidic conditions appeared to enhance sorptive fractionation. The results from this study demonstrate that the importance of sorptive fractionation varies with DOM composition and other factors, and that non-selective sorption can contribute substantially to the formation of mineral-organic associations.

Keywords: soil organic matter; dissolved organic carbon; dissolved organic nitrogen; sorption; adsorption; iron; clay; sewage sludge; FT-ICR MS

1. Introduction

Soils are composed of mineral matter, natural organic matter, and voids that are filled with air, water, or both. Soil constituents are transformed under the influence of biota, climate, topography, and other factors to produce cohesive aggregates of soil materials, a range of chemical environments (e.g., reducing and oxidizing) [1,2], and diverse microenvironments teeming with life. Soils have been called the most complicated biomaterial on Earth, and are heterogeneous across all measured scales, from nm to km [3]. Soils contain far more carbon than vegetation and the atmosphere combined [4], evidencing both that carbon turnover times in soils are relatively long, and that soil organic matter plays a key role in terrestrial carbon cycling. Other important soil organic matter functions include

increasing water retention, improving soil structure and aeration, providing nutrients for plant growth, and sequestering contaminants [5,6].

The natural organic matter in soils is derived primarily from plants and microbes [7,8]. Biotic and abiotic processes transform the precursor molecules to various degrees, producing an extremely complex mixture of organic molecules with almost a continuous range of properties and reactivities [9]. Natural organic matter is most abundant in litter layers and upper mineral horizons, and is transported to subsoils in water as dissolved molecules and fine suspended colloids (collectively, “dissolved organic matter” or “DOM”) [10,11]. DOM concentrations decrease with depth due to degradation and the formation of mineral-organic associations [12–14]. As a result, most of the DOM produced in terrestrial ecosystems is mineralized or retained in soils [10].

Mineral-organic associations comprise organic matter that is sorbed to minerals or trapped in micro-aggregates [12,13] and co-precipitates [15,16]. The amount of organic matter in such associations varies among soil types, and even among horizons within the same soil [12]. Because mineral-organic associations account for up to 91% of total soil carbon, and have carbon turnover times that average four times longer than free or occluded organic matter [13], a comprehensive understanding of the formation and chemical composition of mineral-organic associations would provide important insights into many soil organic matter functions.

According to the zonal model proposed by Kleber et al. [17], organic matter self-assembles on mineral surfaces in a sequence composed of a “contact zone” at the mineral surface, a “hydrophobic zone” in the middle, and a “kinetic zone” at the organic matter-solution interface where organic matter is loosely retained and exchangeable. This implies that mineral-organic associations include a range of chemical and physical interactions that are not confined to mineral surfaces. In support of this model, Solomon et al. [18] observed a wide range of organic carbon functionalities and inorganic components at the organo-mineral interface, and carbon repository zones that were spatially and compositionally distinct, when examining mineral-organic associations with synchrotron-based scanning x-ray transmission microscopy coupled to near edge x-ray absorption fine structure spectroscopy (STXM-NEXAFS). They suggested that no single binding mechanism could explain mineral-organic associations. Similarly, the combination of chemical force spectroscopy with Fourier transform ion cyclotron resonance mass spectrometry (FT-ICR MS) has revealed that different DOM components adhere to iron oxide surfaces with different strengths [19]. Also, Comprehensive Multiphase nuclear magnetic resonance (NMR) spectroscopy has demonstrated that soil organic matter includes a rigid, hydrophobic interior and a gel-like, hydrated exterior [20]. Finally, nano-scale secondary ion mass spectrometry (NanoSIMS) has shown that new organic matter preferentially attaches to pre-existing mineral-organic associations [21].

On the other hand, carbon accumulation in soils is limited [22,23], and numerous studies have reported the selective fractionation of natural organic matter during sorption to metal oxides and clay minerals [24–27]. This implies that the formation and the chemical composition of mineral-organic associations are influenced by interactions between mineral surfaces and specific DOM components. Recently, Fleury et al. [28] used high resolution Orbitrap mass spectrometry (MS) with batch-equilibrium sorption experiments to examine the selective fractionation of DOM by alumina (an aluminum oxide) and kaolinite (a 1:1 clay with permanently non-charged surfaces). They demonstrated that sorptive fractionation was mineral type-dependent. Specifically, the kaolinite exhibited weak selectivity, which the authors attributed to nonselective hydrogen bonding, and the alumina exhibited strong selectivity for polycyclic aromatic and oxygen-rich compounds, which they attributed to hydrophobic effects and ligand exchange reactions. Similarly, Lv et al. [29] used FT-ICR MS with batch-equilibrium sorption experiments to examine the sorptive fractionation of peat leachates by iron oxides. They observed comparatively weak sorptive fractionation by goethite and lepidocrocite, and strong sorptive fractionation by ferrihydrite, including the preferential sorption of DOM constituents with high O/C ratios, high double-bond equivalent (DBE) values, and low H/C ratios. Finally, Avneri-Katz et al. [30] used FT-ICR MS, resin fractionation, and batch-equilibrium

sorption experiments to examine the sorptive fractionation of DOM from composted biosolids by a mineral soil, and demonstrated that sorptive fractionation was concentration-dependent. Specifically, unsaturated, oxygen-rich DOM components preferentially sorbed to the mineral soil, and selectivity decreased with increasing concentration.

The objective of this study was to examine the role of sorptive fractionation in associations between DOM from composted biosolids (hereafter, “anthropogenic DOM”) and Fe(III)-montmorillonite, a 2:1 clay with permanently charged surfaces. FT-ICR MS simultaneously resolves and determines the molecular formulas of thousands of constituents per sample, thus permitting a molecular-level qualitative examination of the differences in complex mixtures such as DOM [31]. We combined FT-ICR MS with novel data analysis techniques to compare the compositions of DOM with the compositions of organic matter sorbed during batch-equilibrium experiments. To examine the influence of DOM composition, we used resin-based separation to produce DOM subsamples with different molecular compositions and chemical properties, separated by hydrophobicity and acidity, and compared the sorption and sorptive fractionation of each structural fraction. We hypothesized that the amount of sorbed organic carbon, and the strength of sorptive fractionation, would depend on the composition of the initial DOM solutions. In particular, we expected the hydrophobic acid (HoA) fraction, which generally contains high carboxyl content [32,33], to sorb most due to the potential for cation bridging and ligand exchange interactions [34,35]. We also expected the samples with the greatest proportion of aromatic and oxygen-rich DOM components to fractionate most. Finally, we hypothesized that the sorbed organic matter would be similar in every experiment due to sorptive fractionation, notwithstanding substantial differences among the initial DOM solutions.

2. Materials and Methods

2.1. Sorbent Preparation

Wyoming Na⁺-montmorillonite (SWy, cation exchange capacity = 76.4 meq/100 g) was obtained from the Clay Minerals Society (Chantilly, VA, USA). The <2 μm fraction of SWy was collected by sedimentation with deionized water and enriched with Fe^(III), as described by Olshansky et al. [36]. In brief, 6 g aliquots of the <2 μm SWy fraction were agitated with 180 mL of 0.3 M FeCl₃ for 2 h at 200 rpm. Next, the SWy was centrifuged at 15,000 g for 10 min, the supernatant was discarded, and the wash procedure was repeated with a fresh FeCl₃ solution. After four sequential washes, the Fe-enriched SWy fraction (Fe(III)-montmorillonite) was dialyzed against deionized water in 12–14 K molecular weight cut-off dialysis bags (Medicell International LTD., London, UK) until the dialysate’s electrical conductivity and chloride concentration were negligible. The pH of the Fe(III)-montmorillonite suspensions was approximately 3.5, limiting the formation of a separate iron oxide mineral phase [37,38]. After preparation, the Fe(III)-montmorillonite was freeze dried and stored in a desiccator.

2.2. DOM Extraction and Fractionation

Structural fractions of the anthropogenic DOM were prepared as described by Avneri-Katz et al. [30]. In brief, DOM was extracted from commercially available composted biosolids (Kfar Menachem, Dlila Facility, Israel; 50% sewage sludge, 50% tree clippings) by overnight agitation at 200 rpm with a 1:10 (w:v) compost to water ratio. The tree clippings are a carbon source [39], and a bulking agent that absorbs moisture and improves aeration during composting [40]. The resulting suspension was centrifuged at 17,000 g for 20 min and filtered through a 0.45 μm Acrodisc Supor membrane (PALL Corp., Ann Arbor, MI, USA). A portion of the resulting anthropogenic DOM was freeze-dried and stored in a desiccator for comparison with the structural fractions.

To produce the structural fractions, the remaining anthropogenic DOM was acidified to pH 3 with 6 M HCl and loaded onto a glass column containing Supelite DAX-8 resin (Supelco, Bellefonte, PA, USA), which selectively retains the hydrophobic fraction [32,41]. The hydrophobic acid (HoA) fraction

was recovered from the DAX-8 resin with 0.1 M NaOH, and the hydrophobic neutral (HoN) fraction was recovered by Soxhlet extraction with methanol for 24 h. The HoN fraction was not recovered in sufficient quantities for replicate experiments. The unretained hydrophilic fraction was loaded sequentially onto glass columns containing cation-exchange (Amberlyst® 15) and anion-exchange (Amberlyst® A21) resins to retain the hydrophilic base (HiB) and hydrophilic acid (HiA) fractions, which could not be recovered in sufficient quantities for further experimentation. The unretained eluent comprised the neutral (HiN) fraction. After preparation, all of the recovered structural fractions were freeze-dried and stored in a desiccator.

2.3. Sorption Experiments

To examine the influence of DOM composition on sorption and sorptive fractionation, batch-equilibrium sorption experiments were conducted using the Fe(III)-montmorillonite, DOM structural fractions, and unfractionated anthropogenic DOM.

To prepare DOM solutions for the sorption experiments, the freeze-dried DOM extracts were dissolved in a background solution prepared with DDW and chloride salts (cations = Ca, K, Mg, and Na, I = 2 mM) to simulate the ionic strength and composition of the original extract from composted biosolids. Prior to DOM addition, the Fe(III)-montmorillonite was agitated in the same background solution at a suspension concentration of 15 g L⁻¹ for 2 h at 200 rpm. Next, the DOM solutions were added to the Fe(III)-montmorillonite suspension to produce 3 g L⁻¹ clay suspensions with the initial organic C concentrations presented in Table 1. The pH of the resulting samples was approximately 3.5. The resulting samples were agitated at 200 rpm for 48 h at 25 °C, based on preliminary kinetics experiments. After equilibration, the samples were centrifuged at 17,000 g for 10 min, and the supernatants were decanted. Following sedimentation, the Fe(III)-montmorillonite samples were washed with DDW to remove unbound DOM, and the sorbed organic matter was extracted from the mineral-organic associations by agitation with 0.1 M NaOH at a suspension concentration of 15 g L⁻¹ for 2 h at 200 rpm. The resulting extracts (each, a “sorbed OM extract”) were filtered through a 0.45-µm filter, and were loaded onto a cation-exchange resin (Amberlyst 15), activated with hydrochloric acid (H⁺), to remove excess sodium.

Table 1. Initial and sorbed carbon amounts (mean ± std, *n* = 6) from the batch equilibrium experiments with 3 g L⁻¹ Fe(III)-montmorillonite, the anthropogenic DOM, and each structural fraction. Sorbed DOC (%) = 3 g dry clay/L × Sorbed DOC (mg C/g dry clay) ÷ Initial DOC (mg C/L). The HoN fraction was not recovered in sufficient quantities for replicate experiments.

Fraction	Initial DOC (mg C/L)	Sorbed DOC (mg C/g dry clay)	Sorbed DOC (%)
Anthropogenic DOM	54 ± 1	9.8 ± 0.4	54 ± 2
HoA Fraction	55 ± 0.9	11.8 ± 0.5	64 ± 3
HoN Fraction	39	7.6	58
HiN Fraction	14 ± 2	2.1 ± 0.2	45 ± 4

The original DOM solutions and the sorbed OM extracts were examined by total organic carbon (TOC) analysis (VCPH model TOC analyzer, Shimadzu Scientific Instruments, Kyoto, Japan) to determine the masses and the proportions of organic carbon that sorbed to the Fe(III)-montmorillonite during the batch-equilibrium experiments (Table 1). The samples were also analyzed by FT-ICR MS to examine their compositions before and after sorption.

2.4. FT-ICR MS Analysis

2.4.1. Sample Preparation

All of the samples were prepared for FT-ICR MS analysis by solid phase extraction (SPE) following the procedure described by Dittmar et al. [42] and Li et al. [43], with some modifications. In brief, 1 g,

6 mL Bond Elut PPL cartridges (Agilent Technologies, Santa Clara, CA, USA) were conditioned with 18 mL of HPLC grade methanol (Sigma-Aldrich, Rehovot, Israel), followed by 30 mL of 0.01 M HCl. Each DOM sample was acidified to pH ~2.5, and loaded onto the SPE cartridges at masses ≤ 10 mg C. Following sample loading, the SPE cartridges were washed with 12 mL of 0.01 M HCl and dried under N₂ for 3–5 min. Next, the DOM was eluted with 2 mL of HPLC grade methanol, freeze-dried, and stored in a desiccator. Immediately prior to analysis, the freeze-dried DOM samples were dissolved in a 50:50 (*v/v*) HPLC grade methanol:DDW solution containing 1% (by volume) NH₄OH to enhance the deprotonation of acidic species for negative ion mode electrospray ionization (ESI⁻).

2.4.2. Instrumental Analysis

The samples were analyzed with a custom-built passively shielded 9.4 T FT-ICR mass spectrometer [44], equipped with a modular software package for data acquisition (Predator) [45]. Negative ions were generated at atmospheric pressure and were transferred into the mass spectrometer by a tube lens/skimmer at 250 V. The ions were accumulated in an RF-only external quadrupole [46], passed through a mass resolving RF-only quadrupole, and collisionally cooled with helium gas ($\sim 3.5 \times 10^{-6}$ Torr) before transfer by octupole ion guides with capacitively coupled excitation electrodes into a seven-segment cylindrical cell [47,48]. A broadband frequency-sweep (“chirp”) excitation (~ 70 to 720 kHz, 50 Hz/ μ s sweep rate, 350 V_{p-p} amplitude) was used for detection. For each sample, 100 time domain transients were coadded, zero-filled, apodized, fast Fourier transformed, and phase-corrected to yield an absorption-mode mass spectrum [49]. The ICR frequencies were converted to *m/z* using a two-term calibration equation based on quadrupolar trapping potential approximation [50,51]. Peak lists were constructed from peaks of magnitude at least six times greater than the standard deviation of the baseline noise (6σ). Next, the spectra were internally calibrated by a “walking” calibration using the most abundant homologous ion series [52].

2.4.3. Data Analysis

Custom software (PetroOrg[®]) was used for additional calibration and elemental composition assignment [53]. The *m/z* values were converted to the Kendrick mass scale [54], assigned an elemental composition (C₁₋₁₀₀ H₄₋₂₀₀ N₀₋₅ O₀₋₂₀ S₀₋₁), and grouped by heteroatom class (O₀N_nS_s) [55]. For each elemental composition, a modified aromaticity index (ModAI) was computed according to Koch and Dittmar [56]. To compare the structural fractions by composition, principal component analysis was performed on selected categories of the FT-ICR MS data using R software (version 3.4.0) [57] and the FactoMineR package [58].

3. Results

3.1. Sorption by Mass

The amounts and proportions of organic carbon that sorbed to the Fe(III)-montmorillonite are presented in Table 1. The original anthropogenic DOM (54 mg C L⁻¹) and original HoA fraction (55 mg C L⁻¹) contained more organic carbon than the original HoN fraction (39 mg C L⁻¹), and more than 3.5 times the organic carbon in the original HiN fraction (14 mg C L⁻¹). The proportions of organic carbon that sorbed to the Fe(III)-montmorillonite, ordered from most to least, were: HoA fraction (64 ± 3%) > HoN fraction (58%) > anthropogenic DOM (54 ± 2%) > HiN fraction (45 ± 4%). The HiN fraction appeared to exhibit unique sorption behavior, because the amount of sorbed organic matter (mg C/g clay) is usually a linear or decreasing function of DOM concentration (mg C L⁻¹), but the HiN fraction sorbed least on a proportionate basis (45 ± 4%) with the lowest concentration (14 mg C L⁻¹).

3.2. Presence of “Surfactant-Like” Peaks

When the composition of the original and sorbed organic matter samples were examined by FT-ICR MS, several series of “surfactant-like” peaks were evident. Using the Kendrick mass scale [54,55], which assigns the same Kendrick mass defect (KMD) to groups of molecules that differ in elemental composition only by one or more $-\text{CH}_2-$ groups (i.e., by alkyl chain length), several sulfur-containing Kendrick series were identified. The surfactant-like series were present in all of the samples, but much less abundant in the sorbed OM extracts (e.g., Supplementary Materials Figure S1). This suggested both that the surfactant-like series were not preferentially sorbed, and that their presence was not caused by laboratory contamination. When the surfactant-like series were highly abundant, ion suppression limited the number of other peaks that could be detected and assigned elemental compositions. As a result, fewer formulas were assigned to the original DOM solutions than their sorbed OM extracts. This was particularly evident in the HoA fraction, when the surfactant-like series were especially abundant.

3.3. Composition-Dependent Sorptive Fractionation

To examine composition-dependent sorptive fractionation, we used FT-ICR MS to identify the formulas that were present both in the original DOM solution and its corresponding sorbed OM extract, and then normalized them to 100% in each sample (hereafter, “Common Formulas”). Formulas that were unique to the original DOM solution or its corresponding sorbed OM extract, due to differences in ion suppression or any other cause, were excluded to ensure that changes in percent abundance were attributable to sorption, and not to differences in the number of assigned formulas. The surfactant-like series were excluded from both samples because they were highly abundant in the original DOM solutions, and much less abundant in the sorbed OM extracts. Without exclusion, they would have dominated the composition of the original DOM solutions, and would have caused the abundances of most other DOM components to appear enhanced in the sorbed OM extracts, masking their sorption behavior relative to each other. The sorption behavior of the surfactant-like series was clear: they tended to remain in solution.

For each sample, the median, mean, and standard deviation of the absolute errors (ppm) of the Common Formula assignments are set forth in Supplementary Materials Table S1. No Common Formula assignment had an absolute error greater than 1 ppm, and no sample had a mean absolute error greater than 0.07 ppm. Except for the HiN fraction (87%), more than 98% of the formulas identified in the original DOM solutions were also identified in their respective sorbed OM extracts. This indicated that the formula assignments for relatively abundant, “unsuppressed” peaks were reproducible, and that most of the identified components in the original DOM solutions were sorbed to the Fe(III)-montmorillonite, at least to some extent. These percentages, like the TOC analysis, suggested that the HiN fraction exhibited unique sorption behavior.

3.3.1. Composition of the Structural Fractions

The van Krevelen diagrams (H/C vs. O/C) in Figure 1 demonstrate that resin-based fractionation produced structural fractions with different molecular compositions, including different relative abundances in the same plot regions. To highlight the Common Formulas that contributed most to the composition of each original sample, the Common Formulas were ranked from most to least abundant and divided into quartiles. The “Top 25%” (dark blue in Figure 1), totaling ~25% of the sample’s cumulative abundance, comprised the most abundant Common Formulas. The “Bottom 25%” (light green in Figure 1), also totaling ~25% of the sample’s cumulative abundance, comprised the least abundant Common Formulas. Viewed differently, the Top 25% comprised the smallest proportion, and the Bottom 25% comprised the largest proportion, of the total number of Common Formulas in each sample (Supplementary Materials Figure S2). All of the Common Formulas with a ModAI > 0.5 were designated aromatic (AROM) in accordance with Koch and Dittmar [56], and all of the formulas

with H/C ratios ≥ 1.5 were designated aliphatic (ALIPH), in accordance with Lv et al. [29] and D'Andrilli et al. [59]. Among the structural fractions, the area of greatest abundance (dark blue in Figure 1) varied, notwithstanding substantial overlap in the center of the van Krevelen diagrams.

To examine the composition of the structural fractions in greater detail, we divided the van Krevelen diagrams into nine discreet regions, illustrated in Supplementary Materials Figure S3, and performed a principal component analysis (PCA) using the samples' cumulative percent abundance in each region (Supplementary Materials Table S2). Specifically, the van Krevelen diagram was divided into aliphatic (ALIPH), aromatic (AROM), and mid saturation (MS) regions, and these regions were subdivided by the degree of oxygenation ("LO" = low oxygen content, $O/C \leq 0.3$; "MO" = mid oxygen content, $0.3 < O/C \leq 0.6$; "HO" = high oxygen content, $O/C > 0.6$). These categories were created to avoid describing regions of the van Krevelen diagram with reference to lignin, polyphenols and other biomolecules, which can overlap in the same van Krevelen plot region [60,61] and which can become attenuated beyond recognition in natural organic matter [62].

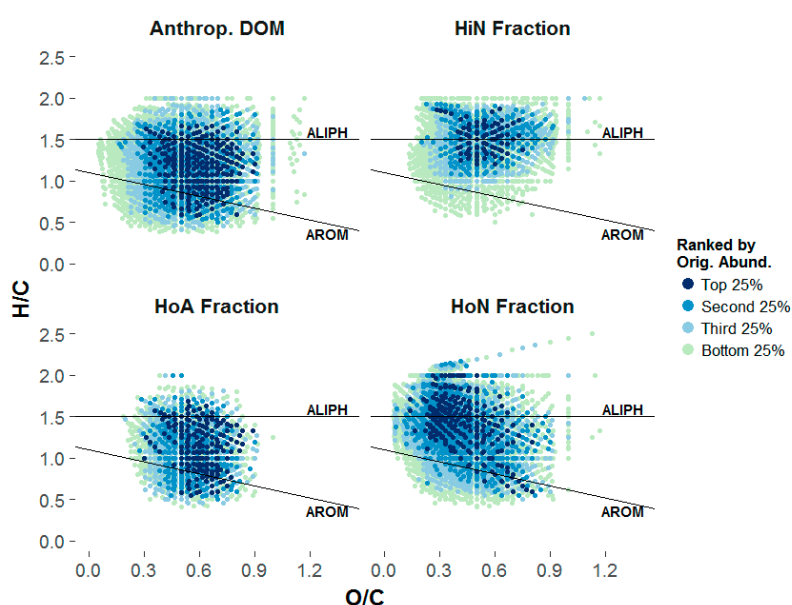


Figure 1. van Krevelen diagrams of the original dissolved organic matter (DOM) solutions. The plotted points represent only the formulas that were present both in the original DOM solution and the corresponding sorbed organic matter extract (Common Formulas). The percent abundances of the Common Formulas in the original DOM solutions were normalized to 100%, ranked from most to least abundant, and divided into quartiles based on their cumulative percent abundances.

According to the PCA (Figure 2), the HoA fraction and the anthropogenic DOM separated from the HiN and HoN fractions along the first principal component ("Dim 1", x axis), primarily because the former group had greater aromatic and MS-HO content, and because the latter group had greater aliphatic content. Along the second principal component ("Dim 2", y axis), the HoN fraction separated from the HiN fraction primarily because the HoN fraction had greater ALIPH-LO and MS-LO content, and because the HiN fraction had greater ALIPH-HO content. The same observations were evident when the cumulative percent abundances of the structural fractions were quantified relative to the anthropogenic DOM in each van Krevelen plot region (Supplementary Materials Figure S4). The HoA fraction did not separate from the anthropogenic DOM in the PCA plots, and differed little from the anthropogenic DOM in Supplementary Materials Figure S4, because their Common Formulas were similarly distributed across the van Krevelen plot regions.

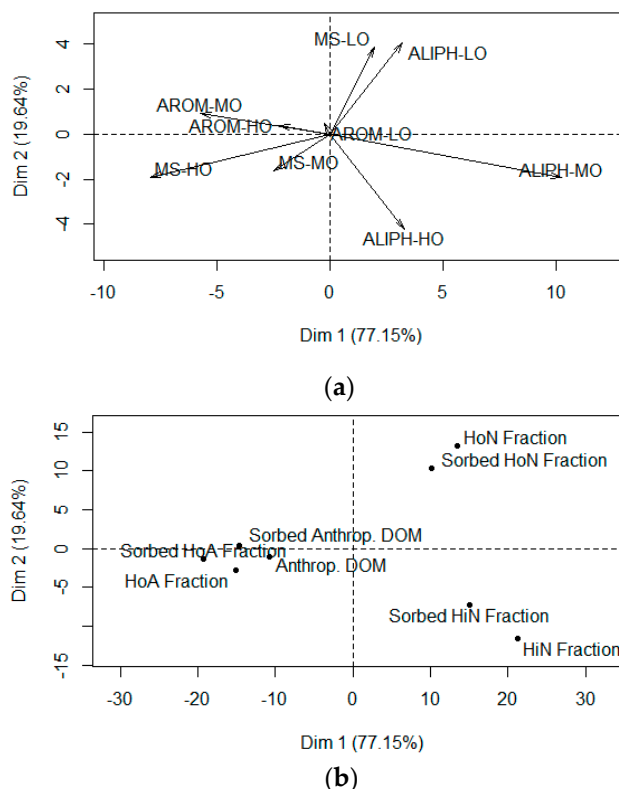


Figure 2. Principal Component Analysis (PCA) plots relating the first and second principal components to (a) the nine van Krevelen plot region variables (Supplementary Materials Figure S3), and (b) the original and sorbed organic matter samples, considering only the formulas that were present in both the original DOM solutions and their corresponding sorbed organic matter extracts (Common Formulas). “ALIPH” = aliphatic ($H/C \geq 1.5$); “AROM” = aromatic ($ModAI > 0.5$); “MS” = mid-saturation ($H/C < 1.5$ and $ModAI \leq 0.5$); “LO” = low oxygen content ($O/C \leq 0.3$); “MO” = mid-oxygen content ($0.3 < O/C \leq 0.6$); “HO” = high oxygen content ($O/C > 0.6$); “ModAI” = modified aromaticity index.

When the Common Formulas from each structural fraction were compared, 5375 Common Formulas were unique to one structural fraction, 1932 Common Formulas were detected in two of the three structural fractions, and 1283 Common Formulas were detected in all three structural fractions (Supplementary Materials Figure S5). Many of the 1283 Common Formulas that were detected in every structural fraction were abundant in the original, unfractionated anthropogenic DOM sample, suggesting that their structural fractionation was incomplete. For example, 319 Common Formulas composed the Top 25% of the original, unfractionated anthropogenic DOM sample, and 301 of them were detected in every structural fraction. Only 155 Common Formulas were unique to the HoA fraction, presumably because the surfactant-like series suppressed and obscured its low abundance peaks, which were most likely to be completely fractionated.

The structural fractions also differed in elemental composition (Supplementary Materials Table S3). The anthropogenic DOM contained elemental classes in the following order of abundance: CHNO (45.6%) > CHO (27.7%) > CHNOS (16.1%) > CHOS (10.6%). Relative to the anthropogenic DOM, the HoA fraction contained less N content (−10.0%), more CHO content (+7.5%), and more CHOS content (+2.5%), presumably because many sulfur-containing surfactant-like compounds were concentrated in the HoA fraction, notwithstanding the removal of the excluded surfactant-like series (as described in Section 3.3). The HiN fraction contained much more CHNO content (+30.1%), and very little CHOS content (1.4%), when compared to the anthropogenic DOM. Finally, the HoN fraction contained much more CHO content (+21.0%), and much less N content (−30.2%), than the anthropogenic DOM.

3.3.2. Sorptive Fractionation

To identify the occurrence of sorptive fractionation, we subtracted the percent abundance of each Common Formula in the sorbed OM extract from its percent abundance in the original DOM solution. A negative result indicated that sorption was favored, and a positive result indicated that sorption was disfavored. Next, we created a seven-category scale (“Most Sorbed” to “Most Unbound”) to describe the degree of sorptive fractionation by the magnitude of the difference in percent abundance (Figure 3). The magnitudes of the individual changes were small, because the total abundance of 100% was divided among thousands of formulas, but the negative and positive results could be summed separately to determine the cumulative compositional changes in each structural fraction (Figure 4a). These cumulative compositional changes were ordered as follows: 32% (HiN fraction) > 18% (HoN fraction) > 14% (HoA fraction) > 10% (anthropogenic DOM).

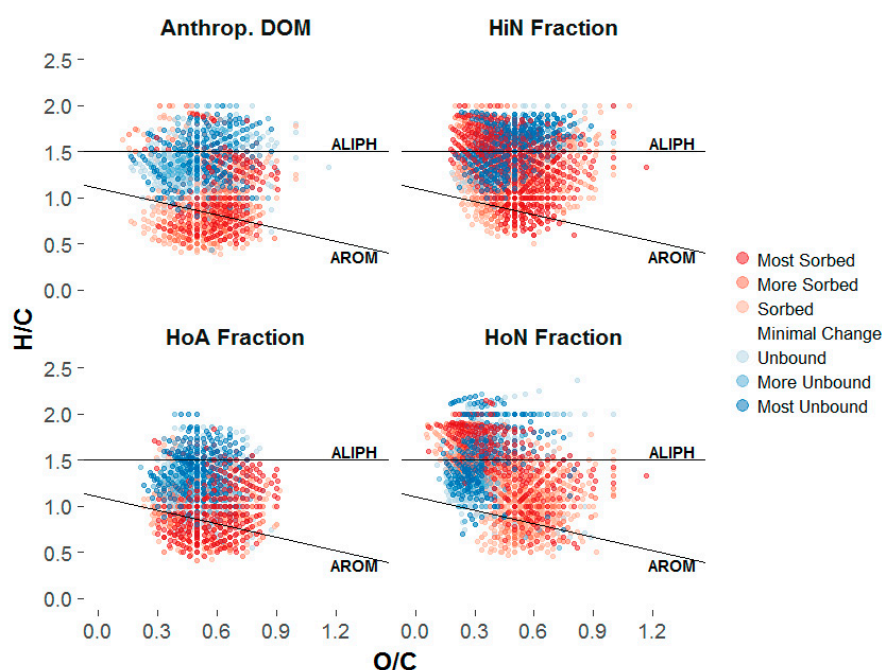


Figure 3. van Krevelen diagrams illustrating the common formulas that were more abundant in the original DOM solutions (Blue), and more abundant in their sorbed organic matter extracts (Red), determined by subtracting the percent abundance of each formula in the sorbed organic matter extract from its percent abundance in the original solution (“Most Sorbed” = Δ abundance < -0.015% ; “More Sorbed” = Δ abundance < -0.010% ; “Sorbed” = Δ abundance < -0.005% ; “Minimal Change”; “Unbound” = Δ abundance > 0.005% ; “More Unbound” = Δ abundance > 0.010% ; “Most Unbound” = Δ abundance > 0.015%).

When the sorption categories were plotted in van Krevelen diagrams (Figure 3), the patterns of sorptive fractionation were apparent. For example, every sample contained ionizable aromatic and oxygen-rich components that preferentially sorbed to the Fe(III)-montmorillonite. To examine the sorptive fractionation in greater detail, the cumulative changes in each sorption category were divided into elemental compositions (Figure 4b) and van Krevelen plot regions (Figure 5).

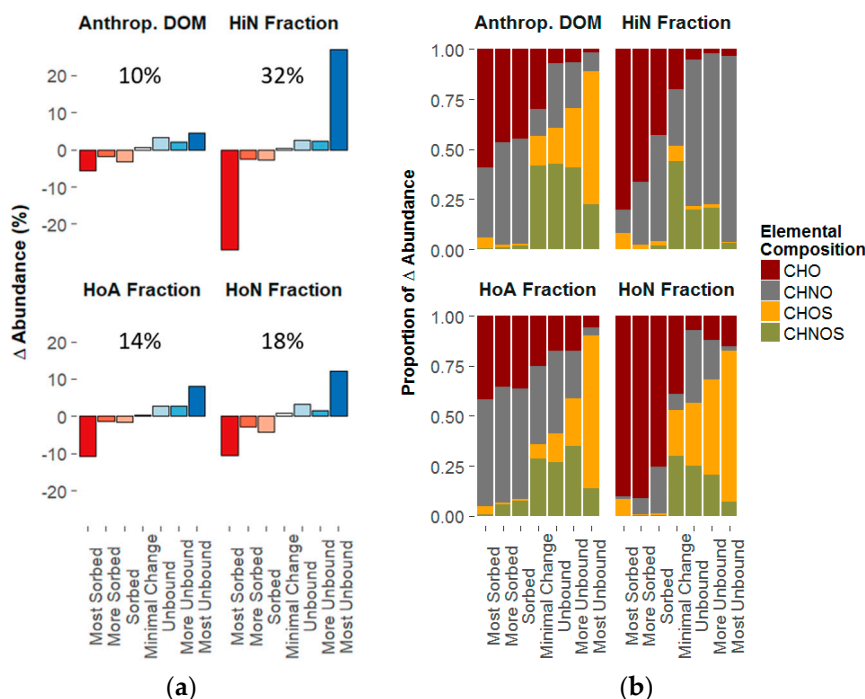


Figure 4. (a) Cumulative changes in percent abundance for the sorption categories described in Figure 3. (b) Distribution of the cumulative changes in percent abundance according to elemental composition (“Most Sorbed” = Δ abundance < -0.015% ; “More Sorbed” = Δ abundance < -0.010% ; “Sorbed” = Δ abundance < -0.005% ; “Minimal Change”; “Unbound” = Δ abundance > 0.005% ; “More Unbound” = Δ abundance > 0.010% ; “Most Unbound” = Δ abundance > 0.015%).

In every sample, the ionizable CHO content preferentially sorbed to the Fe(III)-montmorillonite, and the ionizable sulfur-containing content (CHOS and CHNOS) preferentially remained in solution. In contrast, the ionizable CHNO content exhibited variable sorption behavior. In the HiN fraction, where the CHNO content was greatest (75.8%), the CHNO component mostly remained in solution. In the HoA fraction and anthropogenic DOM, where the sulfur-containing content was greatest, the CHNO component mostly sorbed to the Fe(III)-montmorillonite.

When the sorption categories were examined by van Krevelen plot region, the aromatic and MS-HO regions of every sample, and the ALIPH-LO region of the HiN fraction, mostly sorbed to the Fe(III)-montmorillonite. The other plot regions often split with respect to sorption preference, suggesting heterogeneity within the same plot region. For example, the ALIPH-LO and ALIPH-MO content of the HoN fraction were almost evenly split between “Sorbed” and “Unbound”.

To examine the interactions between elemental composition and van Krevelen plot region in greater detail, the van Krevelen diagrams in Figure 3 were subdivided by elemental composition (Supplementary Materials Figures S6 through S9). The resulting figures suggest that the heterogeneity in the van Krevelen plot regions was primarily driven by elemental composition. For example, in the aliphatic region of the HiN fraction, where the sulfur-containing content was the lowest, the ionizable CHO content preferentially sorbed to the Fe(III)-montmorillonite, and the ionizable CHNO content tended to remain in solution. Alternatively, in the aliphatic region of the HoN fraction, where the CHNO content was the lowest, the ionizable CHO content preferentially sorbed to the Fe(III)-montmorillonite, and the ionizable sulfur-containing content tended to remain in solution.

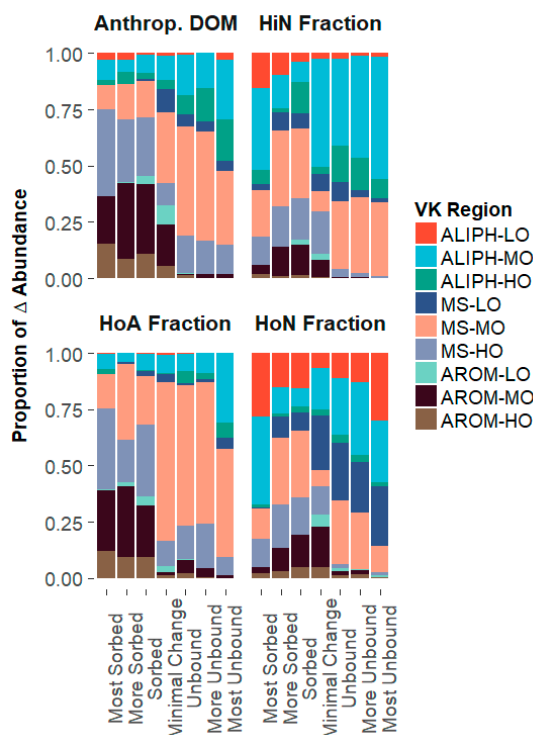


Figure 5. Distribution of the cumulative changes in percent abundance from Figure 4a according to van Krevelen (VK) plot region. “ALIPH” = aliphatic ($H/C \geq 1.5$); “AROM” = aromatic ($ModAI > 0.5$); “MS” = mid-saturation ($H/C < 1.5$ and $ModAI \leq 0.5$); “LO” = low oxygen content ($O/C \leq 0.3$); “MO” = mid-oxygen content ($0.3 < O/C \leq 0.6$); “HO” = high oxygen content ($O/C > 0.6$); “ModAI” = modified aromaticity index.

During the formula assignment, the maximum number of sulfur atoms was one (1), and the maximum number of nitrogen atoms was five (5). To examine the influence of the number of nitrogen atoms on sorption behavior, the ionizable CHNO content in every sample was subdivided by sorption behavior and the number of nitrogen atoms (Figure 6). In almost every case, preferential sorption to the Fe(III)-montmorillonite decreased as the number of nitrogen atoms increased. This behavior was especially prominent in the HiN fraction, which contained the greatest CHNO content (75.8%) and the lowest sulfur-containing content (6.4%). To examine the influence of the number of oxygen atoms on this behavior, the ionizable CHNO content in the HiN fraction was further subdivided by the number of oxygen atoms (Supplementary Materials Figure S10). When the number of nitrogen atoms exceeded one (1), the ionizable CHNO content in the HiN fraction tended to remain in solution, regardless of oxygen content. In contrast, when the number of nitrogen atoms was equal to one (1), the ionizable CHNO content tended to remain in solution when the number of oxygen atoms was less than or equal to six (6), and preferentially sorbed to the Fe(III)-montmorillonite when the number of oxygen atoms was greater than six (6).

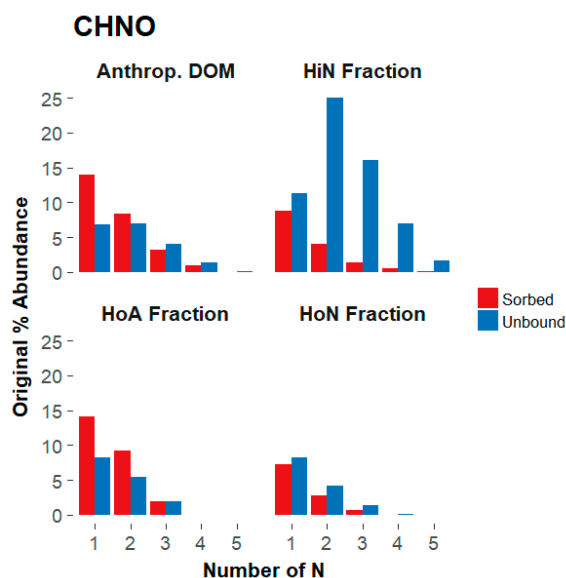


Figure 6. Distribution of CHNO formulas as a function of their original abundance, nitrogen content, and status as “Sorbed” or “Unbound”.

4. Discussion

4.1. Composition-Dependent Sorption

According to the TOC data (Table 1), each structural fraction sorbed to the Fe(III)-montmorillonite to a different extent, supporting our hypothesis that the amount of sorbed organic carbon would depend on the composition of the initial DOM solutions. More specifically, 45 to 64% of the initial organic carbon in every sample sorbed to the Fe(III)-montmorillonite. As expected, the HoA fraction sorbed most (64%), presumably due to its high carboxyl content [32,33], the potential for limited ferrihydrite formation [63], the potential for cation bridging and ligand exchange interactions [34,35], and the acidic conditions of the experiments [64].

4.2. Composition-Dependent Sorptive Fractionation

Two findings were required to demonstrate that DOM composition influenced sorptive fractionation by Fe(III)-montmorillonite: (1) the compositions of the original structural fractions had to be different; and, (2) sorptive fractionation had to vary among the structural fractions.

The structural fractions did exhibit unique molecular compositions (Figure 1), even though the anthropogenic DOM was not completely fractionated (Supplementary Materials Figure S5). For example, the anthropogenic DOM and the HoA fraction had greater aromatic and MS-HO content, and the HiN and HoN fractions had greater aliphatic content (Figure 2). Alternatively, from the perspective of elemental composition, the HoN fraction contained the highest CHO content (48.7%) and the lowest CHNO content (24.6%), while the HiN fraction contained the highest CHNO content (75.8%) and the lowest CHO content (17.8%) (Supplementary Materials Table S3).

Sorptive fractionation is evidenced by changes in composition that occur during sorption. If the composition of the sorbed organic matter differs from the composition of the original DOM solution, then sorptive fractionation has occurred. If its composition is considerably different, then strong sorptive fractionation has occurred.

In this study, a major challenge was to characterize the changes in composition when surfactant-like peaks, which are common to sewage treatment wastewater and biosolids [65–68], suppressed the ionization of constituents in the original DOM solutions. We excluded the surfactant-like series, and focused on the relative abundances of DOM constituents that were both

sorbed to the Fe(III)-montmorillonite and present in the original DOM solutions, where most of the ion suppression was occurring. Using this approach, we could not examine every DOM component that sorbed to the Fe(III)-montmorillonite, but we did characterize changes in the abundances of 87 to 99% of the constituents that were identified in the original DOM solutions. These compositional changes are illustrated in Figure 3 and quantified, as much as possible, in Figure 4a. Using this approach, every sample exhibited sorptive fractionation, and the degree of sorptive fractionation varied, supporting our hypothesis that the strength of sorptive fractionation would depend on the composition of the initial DOM solutions.

On the other hand, Figure 2 illustrates that the sorbed organic matter in every experiment resembled the DOM solution from which it came more than it resembled the sorbed organic matter from the other experiments. This contradicts our hypothesis that all of the sorbed organic matter would be similar due to sorptive fractionation, and suggests that most DOM can be retained in mineral-organic associations, subject to changes in environmental conditions [13,69].

4.3. The Influence of Aromaticity, Oxygen Content, and Nitrogen Content on Sorptive Fractionation

Every sample contained ionizable aromatic and oxygen-rich components that preferentially sorbed to the Fe(III)-montmorillonite (Figure 3), as in previous studies [28–30]. However, those constituents did not determine the strength of sorptive fractionation, contrary to expectations. The greatest compositional change occurred in the HiN fraction (32%), which had low aromatic (1.7%) and MS-HO content (9.0%), and the smallest compositional change occurred in the anthropogenic DOM (10%), which had high aromatic (19.2%) and MS-HO (22.8%) content.

The HiN fraction contained the highest CHNO content (75.8%), which exhibited more sorptive fractionation than any other elemental composition (Figure 4; Supplementary Materials Figures S6 through S9). The HiN fraction also contained the highest ALIPH-MO (35.0%) and ALIPH-HO (15.9%) content, and the lowest aromatic content (1.7%). Aliphatic constituents with more than one nitrogen tended to remain in solution (Figure 6), and aliphatic constituents with one nitrogen split according to the number of oxygens. If the number of oxygens was greater than 6, then the aliphatic constituents preferentially sorbed to the Fe(III)-montmorillonite. Otherwise, the aliphatic constituents tended to remain in solution. We suggest that the strong sorptive fractionation of the HiN fraction was caused primarily by nitrogen-rich, non-aromatic DOM, and that the number of oxygens was only important when the number of nitrogens was low (i.e., 0 or 1).

Acidic conditions produce positively charged basic (e.g., amino) functional groups, uncharged acidic (e.g., carboxyl) functional groups, and positively charged surface hydroxyl groups [70]. Furthermore, montmorillonite facilitates cation bridging interactions if saturated with multivalent cations [25,71]. Under these conditions, DOM constituents with positively charged amino groups would tend to remain in solution, uncharged DOM constituents would tend to sorb through hydrophobic, van der Waals, or hydrogen bonding interactions, and highly acidic [72,73] organic functional groups would tend to participate in ligand exchange or cation bridging interactions [34,35,64]. This could explain strong sorptive fractionation in the HiN fraction. The anthropogenic DOM, HoA fraction, and HoN fraction contained greater CHO content (27.7%, 35.2%, and 48.7%, respectively), and exhibited weaker sorptive fractionation.

Similar behavior has been observed in natural systems. Scott and Rothstein [14] recently determined that nitrogen-rich hydrophilic DOM was weakly retained, when compared to hydrophobic DOM, in soil cores from six forests at pH 4.5 to 6.0. In addition, dissolved organic nitrogen concentrations and C:N ratios commonly increase with soil depth [74].

4.4. The Influence of Non-Selective Sorption on the Formation of Mineral-Organic Associations

Among the structural fractions, the HoA fraction sorbed most (64%), but exhibited the smallest composition change (14%). This suggested that non-selective sorption was important. In fact, every sample appeared to exhibit non-selective sorption because the sorbed organic carbon percentage

(Table 1) always exceeded the cumulative compositional change (Figure 4a). To estimate the relative importance of selective and non-selective sorption in every sample, we compared the cumulative compositional change (Figure 4a) to the sorbed organic carbon percentage (Table 1). If the compositional changes appeared to comprise the primary share of the sorbed organic carbon, then selective sorption was deemed more important. If the compositional changes appeared to comprise a minor share of the sorbed organic carbon, then the opposite was true. On this basis, non-selective sorption was more important than selective sorption in every sample except the HiN fraction, notwithstanding the preferential sorption of aromatic and oxygen-rich DOM in every sample, as in previous studies [28–30]. This supports the zonal model [17], and the suggestion that no single binding mechanism can explain mineral-organic associations [18]. It also supports the suggestion that most DOM constituents can be stabilized in mineral-organic associations.

Other studies have reported multiple binding mechanisms and the sorption of various DOM components to cation-enriched clays. Polubesova et al. [35] used resin-based separation, TOC analysis, UV absorbance spectroscopy, and Fourier transform infrared (FT-IR) analysis with batch equilibrium experiments to examine the sorption of anthropogenic DOM to Cu(II)-montmorillonite, Fe(III)-montmorillonite, and crude montmorillonite. For all clays, the HoN fraction sorbed more than the HoA fraction, and both fractions sorbed to the montmorillonite in the following order: Fe(III)-montmorillonite > Cu(II)-montmorillonite > crude montmorillonite. Sorption of the HoN fraction was attributed to higher hydrophobicity, and sorption of the HoA fraction to the Fe(III)-montmorillonite was attributed to a combination of ligand exchange, van der Waals forces, and hydrogen bonding.

Similarly, Genest et al. [75] combined ^1H high resolution-magic angle spinning (HR-MAS) NMR spectroscopy with batch-equilibrium experiments to examine the sorption of forest soil DOM, Leonardite humic acid, and peat humic acid to Ca^{2+} -enriched kaolinite and montmorillonite. In addition, they used ^1H HR-MAS and solid state ^{13}C NMR spectroscopy to examine whole soils containing kaolinite and montmorillonite. The authors determined that long-chain aliphatic compounds preferentially sorbed to the Ca^{2+} -enriched kaolinite, and that a mixture of aliphatic components and proteins preferentially sorbed to the Ca^{2+} -enriched montmorillonite. In the whole soils, they observed aliphatic components, carbohydrates, and amino acids at the soil–water interface. However, when a more penetrating solvent was used, they also observed aromatic components, implying the existence of hydrophobic, surface-inaccessible domains. Like our study, these findings support the zonal model, and the suggestion that multiple DOM components can be stabilized in mineral-organic associations.

The importance of non-selective sorption is difficult to evaluate during qualitative analyses, which tend to focus on differences in DOM composition. However, the results from this study show that non-selective sorption can contribute substantially to the formation of mineral-organic associations, and thereby influence many soil organic matter functions.

4.5. Additional Environmental Relevance

The use of anthropogenic DOM in this study was environmentally relevant for two reasons. First, composted biosolids are regularly applied to agricultural lands to provide nutrients, enhance soil physical properties, and improve plant yield [76,77]. In the United States, it has been estimated that eight million tons of biosolids are produced each year, and that ~50% is land applied [78]. In addition, Zbytniewski and Buszewski [79] have reported that sewage sludge composting produces organic matter that is structurally similar to soil organic matter. Second, the anthropogenic DOM can serve as a proxy for microbial DOM, which is richer in nitrogen and sulfur-containing constituents than DOM from plant material [80]. In fact, the organic matter in biosolids includes bacterial biomass [81], which might explain the high CHNO content of the anthropogenic DOM.

In addition, the applied experimental conditions were environmentally relevant with respect to acid sulfate soils, which comprise more than 17 million hectares worldwide [82]. These soils form

when sulfide minerals oxidize, producing sulfuric acid and soil pH values < 4. Organic matter addition improves the energy supply for sulfate reducing bacteria, ameliorating the effect of sulfide oxidation, but this improvement depends on the availability of biodegradable organic matter [83,84]. In turn, this availability could be influenced by the formation of mineral-organic associations at low pH.

5. Conclusions

In this study, we combined Fourier transform ion cyclotron resonance mass spectrometry with novel data analysis techniques to examine the role of sorptive fractionation in associations between Fe(III)-montmorillonite and anthropogenic DOM. To examine the influence of DOM composition, we used resin-based separation to produce DOM subsamples with different molecular compositions and chemical properties. A large proportion (45 to 64%) of the initial carbon in every DOM solution sorbed to the Fe(III)-montmorillonite, but each structural fraction sorbed to a different extent, indicating that the amount of sorbed organic carbon depends on DOM composition. Every sample also exhibited sorptive fractionation, and the degree of sorptive fractionation varied, indicating that the strength of sorptive fractionation also depends on DOM composition. Finally, non-selective sorption was more important than selective sorption in every sample except the hydrophilic neutral (HiN) fraction, where high nitrogen content and acidic conditions appeared to enhance sorptive fractionation. This suggests that non-selective sorption can substantially contribute to the formation of mineral-organic associations, and thereby influence a variety of soil organic matter functions.

Supplementary Materials: The following materials are available online at www.mdpi.com/2571-8789/2/1/14/s1: Table S1: Summary statistics for Common Formula assignments; Table S2: Distribution of Common Formulas among van Krevelen plot regions; Table S3: Distribution of Common Formulas among elemental classes; Figure S1: Representative mass spectra for the original and sorbed anthropogenic DOM, before and after exclusion of the surfactant-like series; Figure S2: Distribution of Common Formulas among the quartiles illustrated in Figure 1; Figure S3: Scheme for determining the van Krevelen plot regions; Figure S4: Bar plots demonstrating Common Formula abundances in the van Krevelen plot regions relative to the anthropogenic DOM; Figure S5: Venn diagram illustrating shared Common Formula assignments; Figures S6 through S9: van Krevelen diagrams for each sample illustrating the Common Formulas that were more abundant in the original DOM solutions, and more abundant in their sorbed organic matter extracts, as a function of elemental composition; Figure S10: Bar plots illustrating the status (sorbed or unbound) of the ionizable CHNO content in the HiN fraction as a function of nitrogen and oxygen content.

Acknowledgments: This research was supported by research grants from the U.S. National Science Foundation (grant nos. 1451508 and 1512670), the Israel Science Foundation (grant no. 102/14) and the United States—Israel Binational Agricultural Research and Development Fund (grant nos. US-4551-12 and US-4656-13). The National High Magnetic Field Laboratory is supported by the National Science Foundation Division of Materials Research through DMR-1157490, Florida State University, and the State of Florida.

Author Contributions: B.C., T.B. and T.P. conceived and designed the sorption experiments; S.A.-K. performed the sorption experiments; R.B.Y., A.M.M., H.C. and S.A.-K performed the FT-ICR MS analysis; R.B.Y., A.M.M., H.C., W.B. and S.A.-K. analyzed the data; R.B.Y. and S.A.-K. co-wrote the paper.

Conflicts of Interest: The authors declare no conflict of interest.

References

1. Keiluweit, M.; Nico, P.S.; Kleber, M.; Fendorf, S. Are oxygen limitations under recognized regulators of organic carbon turnover in upland soils? *Biogeochemistry* **2016**, *127*, 157–171. [[CrossRef](#)]
2. Boye, K.; Noël, V.; Tfaily, M.M.; Bone, S.E.; Williams, K.H.; Bargar, J.; Fendorf, S. Thermodynamically controlled preservation of organic carbon in floodplains. *Nat. Geosci.* **2017**, *10*, 415–419. [[CrossRef](#)]
3. Young, I.M.; Crawford, J.W. Interactions and self-organization in the soil-microbe complex. *Science* **2004**, *304*, 1634–1637. [[CrossRef](#)] [[PubMed](#)]
4. Lehmann, J.; Kleber, M. The contentious nature of soil organic matter. *Nature* **2015**, *528*, 60–68. [[CrossRef](#)] [[PubMed](#)]
5. Sparks, D.L. *Environmental Soil Chemistry*; Academic Press: San Diego, CA, USA, 2002.

6. Luthy, R.G.; Aiken, G.R.; Bruseau, M.L.; Cunningham, S.D.; Gschwend, P.M.; Pignatello, J.J.; Reinhard, M.; Traina, S.J.; Weber, W.J.; Westall, J.C. Sequestration of hydrophobic organic contaminants by geosorbents. *Environ. Sci. Technol.* **1997**, *31*, 3341–3347. [[CrossRef](#)]
7. Miltner, A.; Bombach, P.; Schmidt-Brucken, B.; Kastner, M. SOM genesis: Microbial biomass as a significant source. *Biogeochemistry* **2012**, *111*, 41–55. [[CrossRef](#)]
8. Kallenbach, C.M.; Frey, S.D.; Grandy, A.S. Direct evidence for microbial-derived soil organic matter formation and its ecophysiological controls. *Nat. Commun.* **2016**, *7*, 13630. [[CrossRef](#)] [[PubMed](#)]
9. Hertkorn, N.; Frommberger, M.; Witt, M.; Koch, B.P.; Schmitt-Kopplin, P.; Perdue, E.M. Natural organic matter and the event horizon of mass spectrometry. *Anal. Chem.* **2008**, *80*, 8908–8919. [[CrossRef](#)] [[PubMed](#)]
10. Kaiser, K.; Kalbitz, K. Cycling downwards—Dissolved organic matter in soils. *Soil Biol. Biochem.* **2012**, *52*, 29–32. [[CrossRef](#)]
11. Nebbioso, A.; Piccolo, A. Molecular characterization of dissolved organic matter (DOM): A critical review. *Anal. Bioanal. Chem.* **2013**, *405*, 109–124. [[CrossRef](#)] [[PubMed](#)]
12. Kogel-Knabner, I.; Guggenberger, G.; Kleber, M.; Kandeler, E.; Kalbitz, K.; Scheu, S.; Eusterhues, K.; Leinweber, P. Organo-mineral associations in temperate soils: Integrating biology, mineralogy, and organic matter chemistry. *J. Plant Nutr. Soil Sci.-Z. Pflanzenernahr. Bodenkund.* **2008**, *171*, 61–82. [[CrossRef](#)]
13. Kleber, M.; Eusterhues, K.; Keiluweit, M.; Mikutta, C.; Mikutta, R.; Nico, P.S. Mineral-organic associations: Formation, properties, and relevance in soil environments. In *Advances in Agronomy*; Sparks, D.L., Ed.; Elsevier Academic Press Inc.: San Diego, CA, USA, 2015; Volume 130, pp. 1–140.
14. Scott, E.E.; Rothstein, D.E. The dynamic exchange of dissolved organic matter percolating through six diverse soils. *Soil Biol. Biochem.* **2014**, *69*, 83–92. [[CrossRef](#)]
15. Eusterhues, K.; Rennert, T.; Knicker, H.; Kogel-Knabner, I.; Totsche, K.U.; Schwertmann, U. Fractionation of organic matter due to reaction with ferrihydrite: Coprecipitation versus adsorption. *Environ. Sci. Technol.* **2011**, *45*, 527–533. [[CrossRef](#)] [[PubMed](#)]
16. Chen, C.M.; Dynes, J.J.; Wang, J.; Sparks, D.L. Properties of Fe-organic matter associations via coprecipitation versus adsorption. *Environ. Sci. Technol.* **2014**, *48*, 13751–13759. [[CrossRef](#)] [[PubMed](#)]
17. Kleber, M.; Sollins, P.; Sutton, R. A conceptual model of organo-mineral interactions in soils: Self-assembly of organic molecular fragments into zonal structures on mineral surfaces. *Biogeochemistry* **2007**, *85*, 9–24. [[CrossRef](#)]
18. Solomon, D.; Lehmann, J.; Harden, J.; Wang, J.; Kinyangi, J.; Heymann, K.; Karunakaran, C.; Lu, Y.S.; Wirick, S.; Jacobsen, C. Micro- and nano-environments of carbon sequestration: Multi-element STXM-NEXAFS spectromicroscopy assessment of microbial carbon and mineral associations. *Chem. Geol.* **2012**, *329*, 53–73. [[CrossRef](#)]
19. Chasse, A.W.; Ohno, T.; Higgins, S.R.; Amirbahman, A.; Yildirim, N.; Parr, T.B. Chemical force spectroscopy evidence supporting the layer-by-layer model of organic matter binding to iron (oxy)hydroxide mineral surfaces. *Environ. Sci. Technol.* **2015**, *49*, 9733–9741. [[CrossRef](#)] [[PubMed](#)]
20. Masoom, H.; Courtier-Murias, D.; Farooq, H.; Soong, R.; Kelleher, B.P.; Zhang, C.; Maas, W.E.; Fey, M.; Kumar, R.; Monette, M.; et al. Soil organic matter in its native state: Unravelling the most complex biomaterial on Earth. *Environ. Sci. Technol.* **2016**, *50*, 1670–1680. [[CrossRef](#)] [[PubMed](#)]
21. Vogel, C.; Mueller, C.W.; Hoschen, C.; Buegger, F.; Heister, K.; Schulz, S.; Schloter, M.; Kogel-Knabner, I. Submicron structures provide preferential spots for carbon and nitrogen sequestration in soils. *Nat. Commun.* **2014**, *5*, 7. [[CrossRef](#)] [[PubMed](#)]
22. Six, J.; Conant, R.T.; Paul, E.A.; Paustian, K. Stabilization mechanisms of soil organic matter: Implications for C-saturation of soils. *Plant Soil* **2002**, *241*, 155–176. [[CrossRef](#)]
23. Guggenberger, G.; Kaiser, K. Dissolved organic matter in soil: Challenging the paradigm of sorptive preservation. *Geoderma* **2003**, *113*, 293–310. [[CrossRef](#)]
24. Chorover, J.; Amistadi, M.K. Reaction of forest floor organic matter at goethite, birnessite and smectite surfaces. *Geochim. Cosmochim. Acta* **2001**, *65*, 95–109. [[CrossRef](#)]
25. Feng, X.J.; Simpson, A.J.; Simpson, M.J. Chemical and mineralogical controls on humic acid sorption to clay mineral surfaces. *Org. Geochem.* **2005**, *36*, 1553–1566. [[CrossRef](#)]
26. Kramer, M.G.; Sanderman, J.; Chadwick, O.A.; Chorover, J.; Vitousek, P.M. Long-term carbon storage through retention of dissolved aromatic acids by reactive particles in soil. *Glob. Chang. Biol.* **2012**, *18*, 2594–2605. [[CrossRef](#)]

27. Mitchell, P.J.; Simpson, A.J.; Soong, R.; Oren, A.; Chefetz, B.; Simpson, M.J. Solution-state NMR investigation of the sorptive fractionation of dissolved organic matter by alkaline mineral soils. *Environ. Chem.* **2013**, *10*, 333–340. [[CrossRef](#)]
28. Fleury, G.; Del Nero, M.; Barillon, R. Effect of mineral surface properties (alumina, kaolinite) on the sorptive fractionation mechanisms of soil fulvic acids: Molecular-scale ESI-MS studies. *Geochim. Cosmochim. Acta* **2017**, *196*, 1–17. [[CrossRef](#)]
29. Lv, J.; Zhang, S.; Wang, S.; Luo, L.; Cao, D.; Christie, P. Molecular-scale investigation with ESI-FT-ICR-MS on fractionation of dissolved organic matter induced by adsorption on iron oxyhydroxides. *Environ. Sci. Technol.* **2016**, *50*, 2328–2336. [[CrossRef](#)] [[PubMed](#)]
30. Avneri-Katz, S.; Young, R.B.; Mckenna, A.M.; Chen, H.; Corilo, Y.E.; Polubesova, T.; Borch, T.; Chefetz, B. Adsorptive fractionation of dissolved organic matter (DOM) by mineral soil: Macroscale approach and molecular insight. *Org. Geochem.* **2017**, *103*, 113–124. [[CrossRef](#)]
31. Minor, E.C.; Steinbring, C.J.; Longnecker, K.; Kujawinski, E.B. Characterization of dissolved organic matter in Lake Superior and its watershed using ultrahigh resolution mass spectrometry. *Org. Geochem.* **2012**, *43*, 1–11. [[CrossRef](#)]
32. Chefetz, B.; Hatcher, P.G.; Hadar, Y.; Chen, Y.N. Characterization of dissolved organic matter extracted from composted municipal solid waste. *Soil Sci. Soc. Am. J.* **1998**, *62*, 326–332. [[CrossRef](#)]
33. Chefetz, B.; Illani, T.; Schulz, E.; Chorover, J. Wastewater dissolved organic matter: Characteristics and sorptive capabilities. *Water Sci. Technol.* **2006**, *53*, 51–57. [[CrossRef](#)] [[PubMed](#)]
34. Von Lutzow, M.; Kogel-Knabner, I.; Ekschmitt, K.; Matzner, E.; Guggenberger, G.; Marschner, B.; Flessa, H. Stabilization of organic matter in temperate soils: Mechanisms and their relevance under different soil conditions—A review. *Eur. J. Soil Sci.* **2006**, *57*, 426–445. [[CrossRef](#)]
35. Polubesova, T.; Chen, Y.; Navon, R.; Chefetz, B. Interactions of hydrophobic fractions of dissolved organic matter with Fe⁽³⁺⁾- and Cu⁽²⁺⁾-montmorillonite. *Environ. Sci. Technol.* **2008**, *42*, 4797–4803. [[CrossRef](#)] [[PubMed](#)]
36. Olshansky, Y.; Polubesova, T.; Chefetz, B. Reconstitution of cutin monomers on smectite surfaces: Adsorption and esterification. *Geoderma* **2014**, *232*, 406–413. [[CrossRef](#)]
37. Schwertmann, U. Solubility and dissolution of iron oxides. *Plant Soil* **1991**, *130*, 1–25. [[CrossRef](#)]
38. Stefánsson, A. Iron(III) hydrolysis and solubility at 25 °C. *Environ. Sci. Technol.* **2007**, *41*, 6117–6123. [[CrossRef](#)] [[PubMed](#)]
39. Moretti, S.M.L.; Bertoncini, E.I.; Abreu, C.H. Composting sewage sludge with green waste from tree pruning. *Sci. Agricola* **2015**, *72*, 432–439. [[CrossRef](#)]
40. Yanez, R.; Alonso, J.L.; Diaz, M.J. Influence of bulking agent on sewage sludge composting process. *Bioresour. Technol.* **2009**, *100*, 5827–5833. [[CrossRef](#)] [[PubMed](#)]
41. Amery, F.; Vanmoorleghem, C.; Smolders, E. Adapted DAX-8 fractionation method for dissolved organic matter (DOM) from soils: Development, calibration with test components and application to contrasting soil solutions. *Eur. J. Soil Sci.* **2009**, *60*, 956–965. [[CrossRef](#)]
42. Dittmar, T.; Koch, B.; Hertkorn, N.; Kattner, G. A simple and efficient method for the solid-phase extraction of dissolved organic matter (SPE-DOM) from seawater. *Limnol. Oceanogr.-Meth.* **2008**, *6*, 230–235. [[CrossRef](#)]
43. Li, Y.; Harir, M.; Lucio, M.; Kanawati, B.; Smirnov, K.; Flerus, R.; Koch, B.P.; Schmitt-Kopplin, P.; Hertkorn, N. Proposed guidelines for solid phase extraction of Suwannee River dissolved organic matter. *Anal. Chem.* **2016**, *88*, 6680–6688. [[CrossRef](#)] [[PubMed](#)]
44. Kaiser, N.K.; Quinn, J.P.; Blakney, G.T.; Hendrickson, C.L.; Marshall, A.G. A novel 9.4 Tesla FTICR mass spectrometer with improved sensitivity, mass resolution, and mass range. *J. Am. Soc. Mass Spectrom.* **2011**, *22*, 1343–1351. [[CrossRef](#)] [[PubMed](#)]
45. Blakney, G.T.; Hendrickson, C.L.; Marshall, A.G. Predator data station: A fast data acquisition system for advanced FT-ICR MS experiments. *Int. J. Mass Spectrom.* **2011**, *306*, 246–252. [[CrossRef](#)]
46. Senko, M.W.; Hendrickson, C.L.; Emmett, M.R.; Shi, S.D.H.; Marshall, A.G. External accumulation of ions for enhanced electrospray ionization Fourier transform ion cyclotron resonance mass spectrometry. *J. Am. Soc. Mass Spectrom.* **1997**, *8*, 970–976. [[CrossRef](#)]
47. Kaiser, N.K.; Savory, J.J.; Mckenna, A.M.; Quinn, J.P.; Hendrickson, C.L.; Marshall, A.G. Electrically compensated Fourier transform ion cyclotron resonance cell for complex mixture mass analysis. *Anal. Chem.* **2011**, *83*, 6907–6910. [[CrossRef](#)] [[PubMed](#)]

48. Tolmachev, A.V.; Robinson, E.W.; Wu, S.; Kang, H.; Lourette, N.M.; Pasa-Tolic, L.; Smith, R.D. Trapped-ion cell with improved DC potential harmonicity for FT-ICR MS. *J. Am. Soc. Mass Spectrom.* **2008**, *19*, 586–597. [[CrossRef](#)] [[PubMed](#)]
49. Xian, F.; Hendrickson, C.L.; Blakney, G.T.; Beu, S.C.; Marshall, A.G. Automated broadband phase correction of Fourier transform ion cyclotron resonance mass spectra. *Anal. Chem.* **2010**, *82*, 8807–8812. [[CrossRef](#)] [[PubMed](#)]
50. Shi, S.D.H.; Drader, J.J.; Freitas, M.A.; Hendrickson, C.L.; Marshall, A.G. Comparison and interconversion of the two most common frequency-to-mass calibration functions for Fourier transform ion cyclotron resonance mass spectrometry. *Int. J. Mass Spectrom.* **2000**, *195–196*, 591–598. [[CrossRef](#)]
51. Ledford, E.B.; Rempel, D.L.; Gross, M.L. Space charge effects in Fourier transform mass spectrometry—MASS calibration. *Anal. Chem.* **1984**, *56*, 2744–2748. [[CrossRef](#)] [[PubMed](#)]
52. Savory, J.J.; Kaiser, N.K.; Mckenna, A.M.; Xian, F.; Blakney, G.T.; Rodgers, R.P.; Hendrickson, C.L.; Marshall, A.G. Parts-per-billion Fourier transform ion cyclotron resonance mass measurement accuracy with a “walking” calibration equation. *Anal. Chem.* **2011**, *83*, 1732–1736. [[CrossRef](#)] [[PubMed](#)]
53. Corilo, Y.E. *PetroOrg*; The Florida State University: Tallahassee, FL, USA, 2012.
54. Kendrick, E. A mass scale based on $\text{CH}_2 = 14.0000$ for high resolution mass spectrometry of organic compounds. *Anal. Chem.* **1963**, *35*. [[CrossRef](#)]
55. Hughey, C.A.; Hendrickson, C.L.; Rodgers, R.P.; Marshall, A.G.; Qian, K.N. Kendrick mass defect spectrum: A compact visual analysis for ultrahigh-resolution broadband mass spectra. *Anal. Chem.* **2001**, *73*, 4676–4681. [[CrossRef](#)] [[PubMed](#)]
56. Koch, B.P.; Dittmar, T. From mass to structure: An aromaticity index for high-resolution mass data of natural organic matter. *Rapid Commun. Mass Spectrom.* **2006**, *20*, 926–932. [[CrossRef](#)]
57. R Core Team. *R: A Language and Environment for Statistical Computing*; R Foundation for Statistical Computing: Vienna, Austria, 2017.
58. Le, S.; Josse, J.; Husson, F. FactoMineR: An R package for multivariate analysis. *J. Stat. Softw.* **2008**, *25*, 1–18. [[CrossRef](#)]
59. D’andrilli, J.; Cooper, W.T.; Foreman, C.M.; Marshall, A.G. An ultrahigh-resolution mass spectrometry index to estimate natural organic matter lability. *Rapid Commun. Mass Spectrom.* **2015**, *29*, 2385–2401. [[CrossRef](#)] [[PubMed](#)]
60. Kuhnert, N.; Dairpoosh, F.; Yassin, G.; Golon, A.; Jaiswal, R. What is under the hump? Mass spectrometry based analysis of complex mixtures in processed food—Lessons from the characterisation of black tea thearubigins, coffee melanoidines and caramel. *Food Funct.* **2013**, *4*, 1130–1147. [[CrossRef](#)] [[PubMed](#)]
61. Waggoner, D.C.; Chen, H.M.; Willoughby, A.S.; Hatcher, P.G. Formation of black carbon-like and alicyclic aliphatic compounds by hydroxyl radical initiated degradation of lignin. *Org. Geochem.* **2015**, *82*, 69–76. [[CrossRef](#)]
62. Hertkorn, N.; Ruecker, C.; Meringer, M.; Gugisch, R.; Frommberger, M.; Perdue, E.M.; Witt, M.; Schmitt-Kopplin, P. High-precision frequency measurements: Indispensable tools at the core of the molecular-level analysis of complex systems. *Anal. Bioanal. Chem.* **2007**, *389*, 1311–1327. [[CrossRef](#)] [[PubMed](#)]
63. Zhu, M.; Frandsen, C.; Wallace, A.F.; Legg, B.; Khalid, S.; Zhang, H.; Mørup, S.; Banfield, J.F.; Waychunas, G.A. Precipitation pathways for ferrihydrite formation in acidic solutions. *Geochim. Cosmochim. Acta* **2016**, *172*, 247–264. [[CrossRef](#)]
64. Gu, B.H.; Schmitt, J.; Chen, Z.H.; Liang, L.Y.; Mccarthy, J.F. Adsorption and desorption of natural organic matter on iron oxide—Mechanisms and models. *Environ. Sci. Technol.* **1994**, *28*, 38–46. [[CrossRef](#)] [[PubMed](#)]
65. Brunner, P.H.; Capri, S.; Marcomini, A.; Giger, W. Occurrence and behavior of linear alkylbenzenesulfonates, nonylphenol, nonylphenol monophenol and nonylphenol diethoxylates in sewage and sewage sludge treatment. *Water Res.* **1988**, *22*, 1465–1472. [[CrossRef](#)]
66. Gonsior, M.; Zwartjes, M.; Cooper, W.J.; Song, W.; Ishida, K.P.; Tseng, L.Y.; Jeung, M.K.; Rosso, D.; Hertkorn, N.; Schmitt-Kopplin, P. Molecular characterization of effluent organic matter identified by ultrahigh resolution mass spectrometry. *Water Res.* **2011**, *45*, 2943–2953. [[CrossRef](#)] [[PubMed](#)]
67. Cantarero, S.; Prieto, C.A.; Lopez, I. Occurrence of high-tonnage anionic surfactants in Spanish sewage sludge. *J. Environ. Manag.* **2012**, *95*, S149–S153. [[CrossRef](#)] [[PubMed](#)]

68. Schymanski, E.L.; Singer, H.P.; Longree, P.; Loos, M.; Ruff, M.; Stravs, M.A.; Vidal, C.R.; Hollender, J. Strategies to characterize polar organic contamination in wastewater: Exploring the capability of high resolution mass spectrometry. *Environ. Sci. Technol.* **2014**, *48*, 1811–1818. [[CrossRef](#)] [[PubMed](#)]
69. Knorr, K.H. DOC-dynamics in a small headwater catchment as driven by redox fluctuations and hydrological flow paths—Are DOC exports mediated by iron reduction/oxidation cycles? *Biogeosciences* **2013**, *10*, 891–904. [[CrossRef](#)]
70. Tombacz, E.; Libor, Z.; Illes, E.; Majzik, A.; Klumpp, E. The role of reactive surface sites and complexation by humic acids in the interaction of clay mineral and iron oxide particles. *Org. Geochem.* **2004**, *35*, 257–267. [[CrossRef](#)]
71. Arnarson, T.S.; Keil, R.G. Mechanisms of pore water organic matter adsorption to montmorillonite. *Mar. Chem.* **2000**, *71*, 309–320. [[CrossRef](#)]
72. Leenheer, J.A.; Wershaw, R.L.; Reddy, M.M. Strong-acid, carboxyl group structures in fulvic acid from the Suwannee River, Georgia. 1. Minor structures. *Environ. Sci. Technol.* **1995**, *29*, 393–398. [[CrossRef](#)] [[PubMed](#)]
73. Leenheer, J.A.; Wershaw, R.L.; Reddy, M.M. Strong-acid, carboxyl group structures in fulvic acid from the Suwannee River, Georgia. 2. Major structures. *Environ. Sci. Technol.* **1995**, *29*, 399–405. [[CrossRef](#)] [[PubMed](#)]
74. Bingham, A.H.; Cotrufo, M.F. Organic nitrogen storage in mineral soil: Implications for policy and management. *Sci. Total Environ.* **2016**, *551–552*, 116–126. [[CrossRef](#)] [[PubMed](#)]
75. Genest, S.C.; Simpson, M.J.; Simpson, A.J.; Soong, R.; McNally, D.J. Analysis of soil organic matter at the solid-water interface by nuclear magnetic resonance spectroscopy. *Environ. Chem.* **2014**, *11*, 472–482. [[CrossRef](#)]
76. Kinney, C.A.; Furlong, E.T.; Zaugg, S.D.; Burkhardt, M.R.; Werner, S.L.; Cahill, J.D.; Jorgensen, G.R. Survey of organic wastewater contaminants in biosolids destined for land application. *Environ. Sci. Technol.* **2006**, *40*, 7207–7215. [[CrossRef](#)] [[PubMed](#)]
77. Cogger, C.G.; Forge, T.A.; Neilsen, G.H. Biosolids recycling: Nitrogen management and soil ecology. *Can. J. Soil Sci.* **2006**, *86*, 613–620. [[CrossRef](#)]
78. Gray, J.L.; Borch, T.; Furlong, E.T.; Davis, J.G.; Yager, T.J.; Yang, Y.Y.; Kolpin, D.W. Rainfall-runoff of anthropogenic waste indicators from agricultural fields applied with municipal biosolids. *Sci. Total Environ.* **2017**, *580*, 83–89. [[CrossRef](#)] [[PubMed](#)]
79. Zbytniewski, R.; Buszewski, B. Characterization of natural organic matter (NOM) derived from sewage sludge compost. Part 1: Chemical and spectroscopic properties. *Bioresour. Technol.* **2005**, *96*, 471–478. [[CrossRef](#)] [[PubMed](#)]
80. D'andrilli, J.; Foreman, C.M.; Marshall, A.G.; Mcknight, D.M. Characterization of IHSS Pony Lake fulvic acid dissolved organic matter by electrospray ionization Fourier transform ion cyclotron resonance mass spectrometry and fluorescence spectroscopy. *Org. Geochem.* **2013**, *65*, 19–28. [[CrossRef](#)]
81. Jardé, E.; Mansuy, L.; Faure, P. Organic markers in the lipidic fraction of sewage sludges. *Water Res.* **2005**, *39*, 1215–1232. [[CrossRef](#)] [[PubMed](#)]
82. Ljung, K.; Maley, F.; Cook, A.; Weinstein, P. Acid sulfate soils and human health—A Millennium Ecosystem Assessment. *Environ. Int.* **2009**, *35*, 1234–1242. [[CrossRef](#)] [[PubMed](#)]
83. Jayalath, N.; Mosley, L.M.; Fitzpatrick, R.W.; Marschner, P. Addition of organic matter influences pH changes in reduced and oxidised acid sulfate soils. *Geoderma* **2016**, *262*, 125–132. [[CrossRef](#)]
84. Kolbl, A.; Marschner, P.; Fitzpatrick, R.; Mosley, L.; Kogel-Knabner, I. Linking organic matter composition in acid sulfate soils to pH recovery after re-submerging. *Geoderma* **2017**, *308*, 350–362. [[CrossRef](#)]

